Available online at www.sciencedirect.com
ScienceDirect
Trans. Nonferrous Met. Soc. China 32(2022) 104−121
Transactions of Nonferrous Metals Society of China
www.tnmsc.cn

Microstructure, mechanical properties and wear resistance of SiC_p/AZ91 composite prepared by vacuum pressure infiltration

Zhi-ping GUAN[1,2], Ming-yu LI[1,2], Kai-xin XIA[2], Zhi-gang LI[2], Dan GAO[2], Po ZHAO[2], Pin-kui MA[2], Jia-wang SONG[1]

1. State Key Laboratory of Automotive Simulation and Control, Jilin University, Changchun 130022, China;
2. School of Materials Science and Engineering, Jilin University, Changchun 130022, China

Received 22 December 2020; accepted 11 October 2021

Abstract: SiC_p/AZ91 composites were prepared by vacuum pressure infiltration. The microstructure, mechanical properties and wear resistance of composite were studied. Results indicated that SiC particles were uniformly distributed in the metal matrix and had a good interface bonding with the metal matrix. $Mg_{17}Al_{12}$ preferably precipitated near the SiC particles, and high-density dislocations were induced by the mismatch of the coefficient of thermal expansion (CTE) between the SiC particle and the AZ91 matrix, thereby accelerating the aging precipitation of the matrix. Compared with AZ91 alloy, the addition of SiC particles improves the hardness and compressive strength of the composite, which is mainly due to the load transfer strengthening and grain refinement strengthening mechanisms. Furthermore, a stable support surface-protecting matrix formed during the wear process because of the excellent wear resistance of SiC.

Key words: magnesium matrix composites; SiC particle; vacuum pressure infiltration; aging behavior; wear

1 Introduction

Magnesium is one of the lightest metals and has a density of about two-thirds that of aluminum [1]. Magnesium and its alloys have been widely explored in aerospace, automotive and electronic industries [2−4]. Given these properties, they are potential lightweight structural materials for the automotive and aerospace industries [5]. However, magnesium alloys have lower mechanical properties and wear resistance than other light metals. These disadvantages limit the possible applications of magnesium alloys.

To further improve the mechanical strength and wear resistance of magnesium alloys, magnesium-matrix composites were prepared by adding various reinforcements to magnesium matrix, such as ceramic particles (SiC, Al_2O_3, TiC, etc) [6−10], grapheme [11], carbon nanotubes [12] and nano-AlN particles [13]. Among them, SiC particles are low cost and have excellent wear and oxidation resistance. SiC has good wettability with a magnesium matrix and can combine well with the interface [14]. Thus, SiC particle reinforced magnesium matrix composites are also promising.

The processing methods and properties of particle-reinforced magnesium matrix composites have been widely explored. VISWANATH et al [15] synthesized AZ91-SiC_p composites through stir-casting method and studied the mechanical properties and creep behavior of composites. Similarly, GANGULY and MONDAL [16] explored the influence of the addition of SiC nanoparticles on the microstructure and creep behavior of a squeeze-cast AZ91-Ca−Sb magnesium alloy. Experimental results reveal that the mechanical properties and creep resistance of the composites

Corresponding author: Jia-wang SONG, Tel: +86-13159829772, E-mail: songjw@jlu.edu.cn
DOI: 10.1016/S1003-6326(21)65781-3

improve with the addition of reinforcements. RASHAD et al [17] fabricated grapheme nano platelet reinforced AZ61 magnesium alloy through the melt-deposition method. The mechanical properties of composites at room and high temperatures have also been examined. TURAN et al [18] studied the mechanical, tribological, and corrosion properties of fullerene-reinforced magnesium matrix composites fabricated through semi-powder metallurgy. The mechanical properties (i.e., hardness, compression yield, and ultimate strength) of pure magnesium considerably improve with the addition of fullerene. Almost all the research on magnesium matrix composites focuses on the tensile and mechanical properties, but less on the friction and wear resistance. The addition of reinforcement can greatly improve the wear resistance of magnesium alloy. LIM et al [19] investigated the sliding wear behavior of SiC_p/AZ91 composites at loads of 10−30 N. Compared with the matrix alloy, the wear resistance of a composite at a low load of 10 N is significantly improved, with an increase of 15%−30%. GARCÍA-RODRÍGUEZ et al [20] explored the dry sliding wear behavior of globular AZ91 alloy and SiC_p/AZ91 composites. They found that the wear mechanism of globular AZ91 alloy varies under different loads and sliding speeds, and oxidative wear dominates in composites. Studies on the comprehensive mechanical properties of magnesium matrix composites prepared through vacuum pressure infiltration are fewer than those of other preparation methods. Aging behavior can change the existence of the second phase in the AZ91 alloy and improve its microstructure and mechanical properties. SiC reinforcement plays a significant role in alloys [21,22]. ZHENG et al [23] studied the aging hardening kinetics of squeeze cast SiC_w/AZ91 magnesium matrix composite. The addition of SiC to AZ91 alloy induces an accelerated hardening response, and age-hardening efficiency in the composite is low. Reinforcement and age hardening are important in improving matrix properties, but few systematic studies have been conducted on their effects on the mechanical properties of magnesium alloys, especially SiC_p/AZ91 composites.

Vacuum pressure infiltration has a wide range of applications and can be used in the composite of various metal, matrix, and reinforcing materials, including fibers, whiskers, and particles [24,25]. The composites prepared by this method have a compact structure, uniform reinforcement distribution, and good interfacial bonding [26,27].

The purpose of this study is to fabricate SiC particle reinforced magnesium matrix composites with good interface by vacuum pressure infiltration method, and to investigate their comprehensive mechanical properties.

2 Experimental

2.1 Materials

In this study, the as-cast AZ91 alloy was the matrix alloy, and its chemical composition is shown in Table 1. Green and abrasive grade SiC particles with an average diameter of 40 μm were selected as the reinforcements. For preparation of SiC preforms, sodium metasilicate (Na_2SiO_3) powders and polyvinyl alcohol (PVA) powders were used as high temperature adhesives and ambient temperature adhesives respectively, and starch powders were chosen as the pore-forming agents. After heating, the starch was decomposed into CO_2 and H_2O, which overflowed from the preforms, leaving pores in the preform. Na_2SiO_3 had strong adhesion, high strength and good heat resistance, but it was not volatile at high temperatures, so it was available in small quantities. PVA powders are an organic compound that may be decomposed by oxidation at a certain temperature.

Table 1 Chemical composition of AZ91 alloy (wt.%)

Al	Zn	Mn	Fe	Si	Cu	Ni	Mg
8.500	0.800	0.300	0.004	0.050	0.025	0.010	Bal.

2.2 Preparation of SiC preforms

Firstly, SiC particles, Na_2SiO_3 powders, PVA powders and starch powders were evenly mixed with a mass ratio of 10:1:2:2, which is consistent with the theoretical volume fraction (~45%) of SiC, and then the dry mixed powders were stirred to a smooth paste with a little deionized water. Next, the dehydrated mixture was pressed into a cylinder in a mold with an inner diameter of 8 mm. Finally, the preforms were sintered in resistance furnace with the sintering process shown in Fig. 1.

2.3 Vacuum pressure infiltration

Firstly, the preform was placed on the bottom

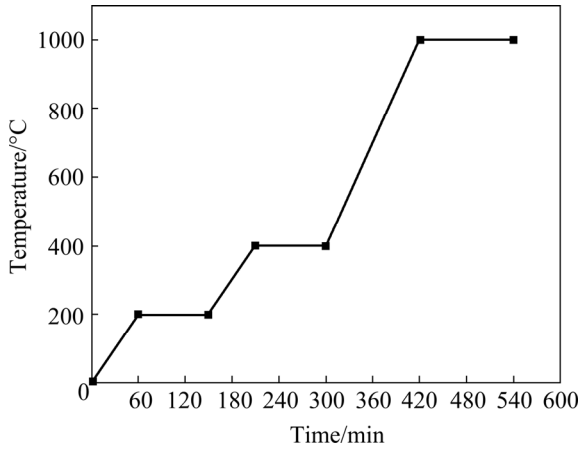

Fig. 1 Sintering curve of preforms

of graphite crucible, and the chunks of AZ91 alloy were spread on the preform. The graphite crucible was vaccum sealed in an alundum tube. The chunks were melted into liquids by heating to 680 °C in a tubular furnace and holding for the shortest time possible, avoiding the volatilization of magnesium element. Then, argon gas was filled into the alundum tube up to an absolute pressure of 250 kPa in order to press the liquid AZ91 alloy into the pores of the preform while thoroughly shaking and mixing it within 10 min. Next, the alundum tube was moved 187 μm from the heating zone of the tubular furnace with upward velocity of 30 mm/min, leading to an elimination of casting defects by directional solidification. Finally, the SiC_p/AZ91 composite was obtained after slow cooling to ambient temperature. The preparation process is presented in Fig. 2.

2.4 Heat treatment

Heat treatment process was given in Ref. [28]. The matrix alloy and composite were solution treated at 415 °C for 24 h. After solution treatment, the alloy and composite were aged at 175 °C for different periods up to 48 h. The aging time of the samples is as follows: 2, 4, 6, 10, 14, 18, 22, 26, 30, 36, 42 and 48 h. The optimum heat treatment scheme was selected by hardness test.

2.5 Characterization

The crystal structure was identified by the poly-crystalline X-ray diffractometer (XRD). Microstructure characterization specimens were prepared by grinding from 400 to 2000 grit paper and metallographically polished with diamond paste. Carl Zeiss Jena scanning electron microscope (SEM) equipped with EDS was used to examine the microstructure of SiC reinforced composite. The three-dimensional morphologies of the SiC_p/AZ91 after wear test were observed by VW−9000 series high-speed digital microscopy system.

The age-hardening response of the composite materials and unreinforced alloy was characterized using HB−3000B Brinell hardness tester. The ratio of diameter to height of the cylindrical compression

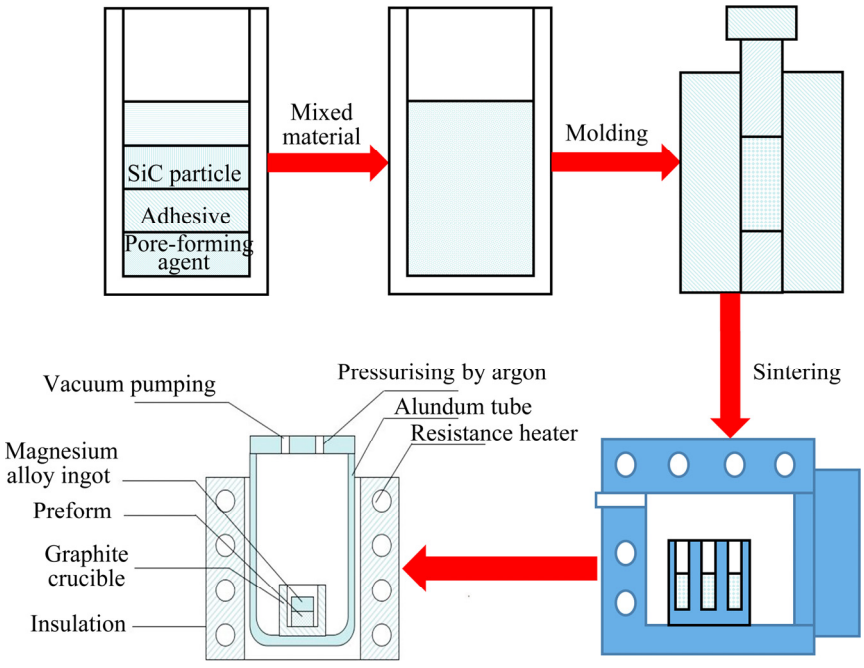

Fig. 2 Fabrication stages of SiC_p/AZ91 composites

sample is 1:2. Room and high temperature compression tests with 1.0 mm/min were conducted by WQ4100 universal test machine. Graphite lubricant was used to reduce the influence of friction on compression experiments. YTN TB−1000 tribometer test machine in a reciprocating contact configuration was used to examine wear properties. The sizes of friction and wear test sample were *d*9 mm × 20 mm. The wear tests were carried out for all samples under loads of 10, 20 and 30 N. The sliding speed was 1.6 m/s and the wear time was 20 min. The counterbody was 40Cr. The specimens for CTE testing with the dimensions of *d*5 mm × 10 mm were machined from the composite rods. The CTE measurements were performed from room temperature to 350 °C at a heating rate of 5 °C/min using a 190−1500*/DIL802* thermal dilatometer.

3 Results

3.1 Material characterization

3.1.1 X-ray diffraction(XRD) results

The XRD patterns of AZ91 alloy and the SiC_p/AZ91 composites before and after heat treatment are shown in Fig. 3, and Fig. 4 presents the heat-treated SiC_p/AZ91 composites. According to the XRD pattern, the AZ91 alloy and the composites contain Mg, SiC, and $Mg_{17}Al_{12}$ eutectic compounds. The peak of the MgO phase is found in the untreated and heat-treated composites (Fig. 3). During drying, SiC was in a high temperature and high humidity environment. The surface of the SiC particles easily oxidized to form SiO_2, which reacted with the molten magnesium alloy to form MgO. A similar result was previously reported [27,29].

3.1.2 Microstructure analysis

Scanning electron microscopy (SEM) was applied to examining the surface morphology of the samples. Figures 5 and 6 show the SEM microstructures of the AZ91 alloy and the SiC_p/AZ91 magnesium matrix composite before and after the solution. Figures 5(a) and (b) illustrate that $Mg_{17}Al_{12}$ primarily precipitates along the grain boundary, and a small amount of the second phase precipitates discontinuously. Figures 5(c) and (d) present SEM images of SiC_p/AZ91 composites. No macrostructural defects in the microstructure are observed, and the distribution of the SiC particles is uniform in the magnesium matrix. With the magnesium matrix, SiC has good wettability [14]. The magnesium alloy melt can fully infiltrate the

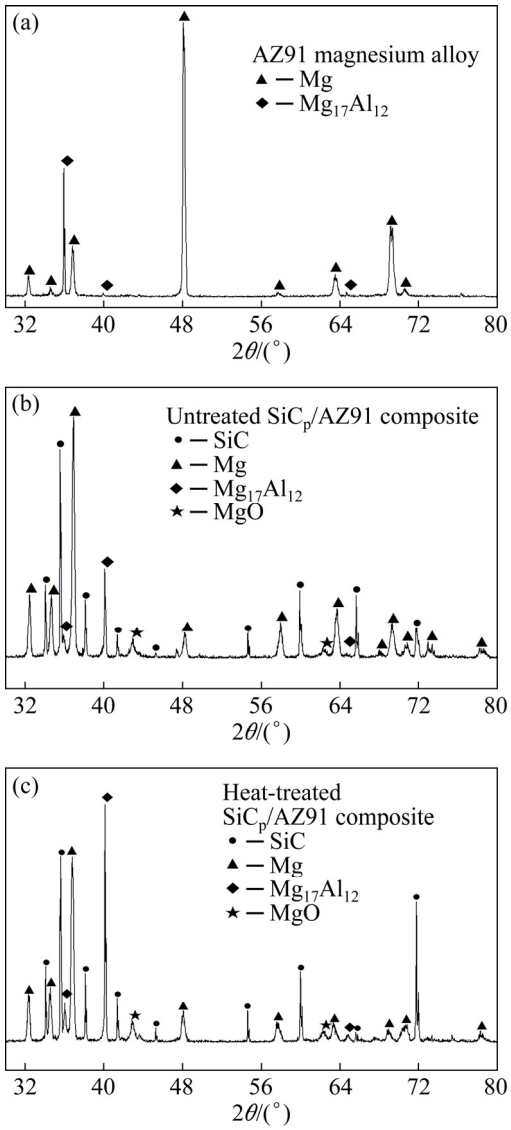

Fig. 3 XRD patterns of AZ91 alloy and SiC_p/AZ91 composite

Fig. 4 Sample of SiC_p/AZ91 composite after heat treatment

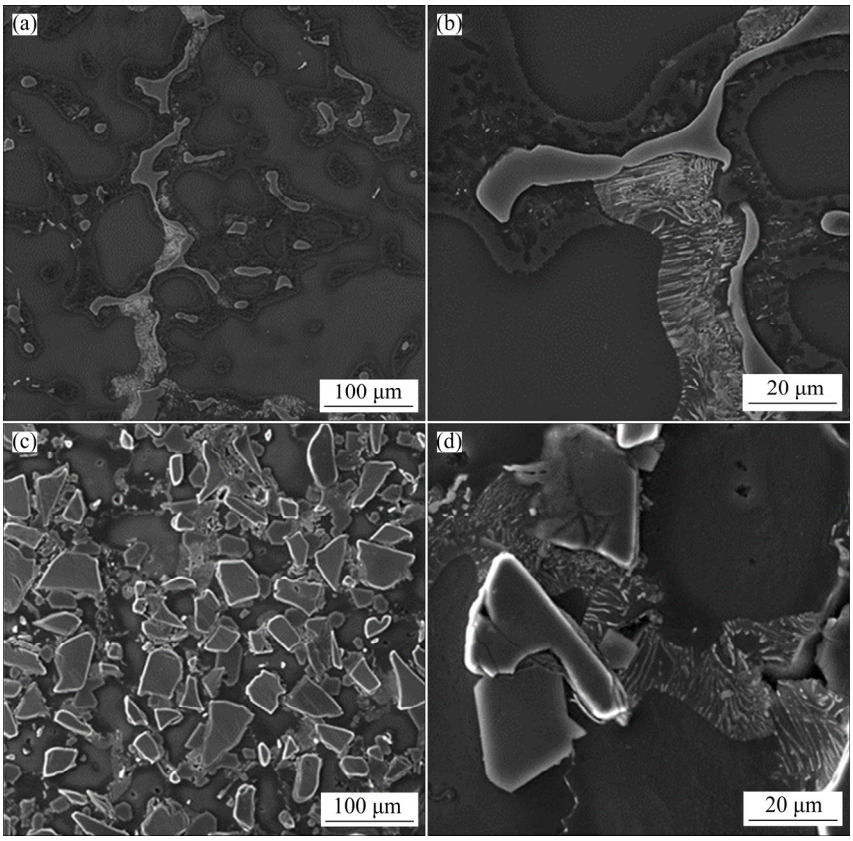

Fig. 5 SEM images of as-cast AZ91 alloy (a, b) and SiC_p/AZ91 composites (c, d)

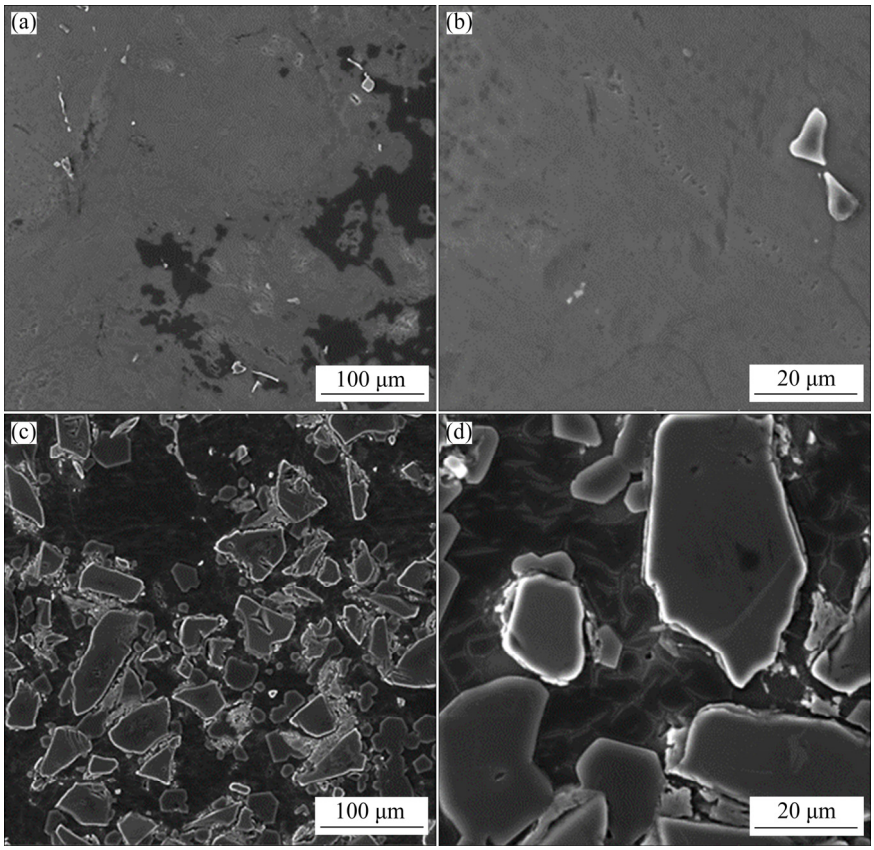

Fig. 6 Microstructures of AZ91 alloy (a, b) and SiC_p/AZ91 composites (c, d) after solid solution treatment: (a, c) Low magnification; (b, d) High magnification

gap between the adjacent SiC particles under the action of vacuum and air pressure, resulting in good bonding between the SiC particles and the magnesium matrix. A small amount of the second phase precipitated discontinuously in the as-cast composite, and the precipitation position was primarily near SiC particles [30]. Moreover, the addition of the SiC particles significantly reduced the grain size of the AZ91 matrix, resulting in the effect of fine-grain strengthening.

Solution treatments should be administered before aging treatment to eliminate the existence of the coarse second phase in solidification. The matrix alloy and composite were solution treated at 415 °C for 24 h. Figure 6 illustrates the microstructures of the as-cast AZ91 alloy and the SiC_p/AZ91 composite after the solution treatment. The coarse $Mg_{17}Al_{12}$ phase in the alloy and the composite decreased obviously. The second phase was not found at the interface between the SiC particles and matrix and the grain boundary of the magnesium matrix.

The influence mechanism of SiC particles on the aging precipitation behavior of the magnesium matrix composites was explored to analyze the microstructure evolution of aging precipitates in SiC_p/AZ91 composites. Figure 7 shows the SEM images of the composite treated at different aging time. At the early stage of aging, as shown in Figs. 7(a) and (b), $Mg_{17}Al_{12}$ preferred to nucleate and grow near the SiC particles, and $Mg_{17}A1_{12}$ precipitates at the grain boundaries were seldom observed. As the aging time further prolonged, as presented in Figs. 7(c) and (d), the amount of precipitates increased greatly; consequently, they covered almost the entire magnesium matrix and mixed with the SiC particles. In Figs. 7(e) and (f), the size of the precipitates grew obviously at the later stage of aging. The precipitates near the SiC particles were larger than those in the other regions, and their morphology was rod shaped. The aging time required for $Mg_{17}Al_{12}$ to cover the entire magnesium matrix and size coarsening shortened compared with those of the magnesium alloy. $Mg_{17}A1_{12}$ preferred to precipitate near SiC particles, and it was easier to nucleate than that at the grain boundary. Therefore, the addition of the SiC particles accelerated the aging precipitation of the matrix.

3.2 Age-hardening response

The effects of aging time on the hardness of the SiC_p/AZ91 composite and the AZ91 alloy treated at 175 °C are shown in Fig. 8. In general, the hardness of both materials showed similar trends, i.e., it peaked and then gradually decreased with prolonging aging time. The hardness of the composite was greatly improved by the SiC particle addition compared with that of the magnesium alloy. However, the time needed to reach the peak hardness is different (36 h for AZ91 alloy and 18 h for SiC_p/AZ91). This finding indicated that SiC particles accelerated the aging kinetics of the magnesium matrix, which was consistent with the age-hardening response in Ref. [28], Thus, the following optimum treatment process of the composite was obtained: solution treatment (415 °C) 24 h + aging treatment (175 °C) 18 h. All the heat-treated composites were subsequently produced under the optimum heat-treatment conditions.

3.3 Analysis of coefficient of thermal expansion (CTE)

Figure 9 shows the CTE as a function of temperature of the AZ91 alloy and the SiC_p/AZ91 composites before and after the heat treatment. Evidently, the CTE of composites was lower than that of the AZ91 alloy. At the same time, the CTE of the AZ91 alloy and its composites increased as temperature increased. These differences were due to the addition of SiC particles. The linear expansion coefficient of SiC is much smaller than that of the magnesium alloy [26,27]. The expansion of SiC should be coordinated with the matrix alloy. SiC reinforcement was elongated by the matrix phase, which was compressed by SiC reinforcement during heating. Thus, the CTE of the composite was far less than that of the magnesium alloy. Figure 9 shows that the CTE of the composite after heat treatment is increased. In the present study, the heat-treated composites were obtained through the optimum heating process: solution treatment (415 °C) for 24 h + aging treatment (175 °C) for 18 h. The effect of heat treatment on the thermal expansion behavior is primarily due to the residual stress after quenching and the precipitation phase of aging. After aging, the reduction in residual stress and the increase in the precipitated phase increased the CTE.

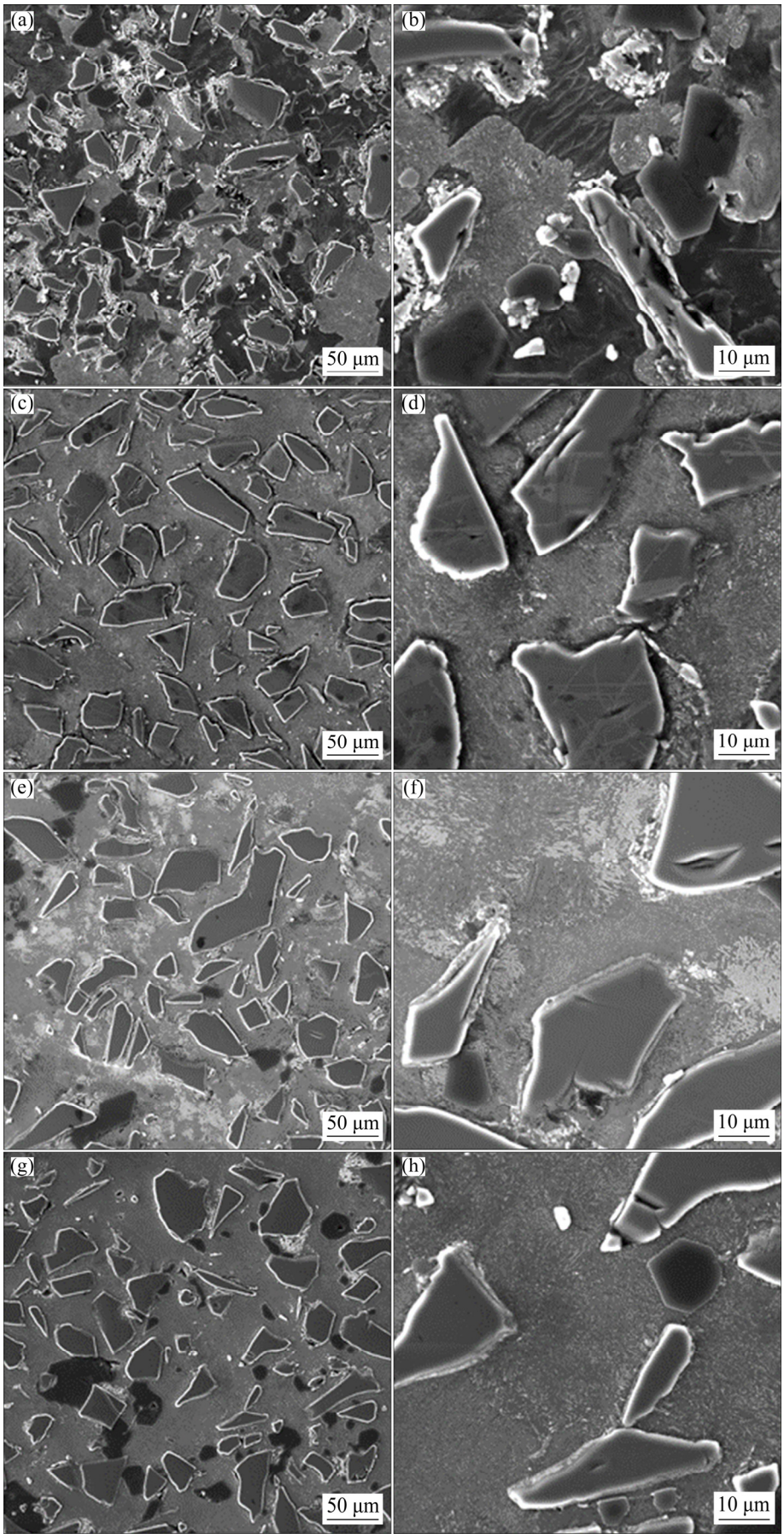

Fig. 7 SEM images of SiC_p/AZ91 composites treated at different aging time: (a, b) 6 h; (c, d) 18 h; (e, f) 36 h; (g, h) 48 h

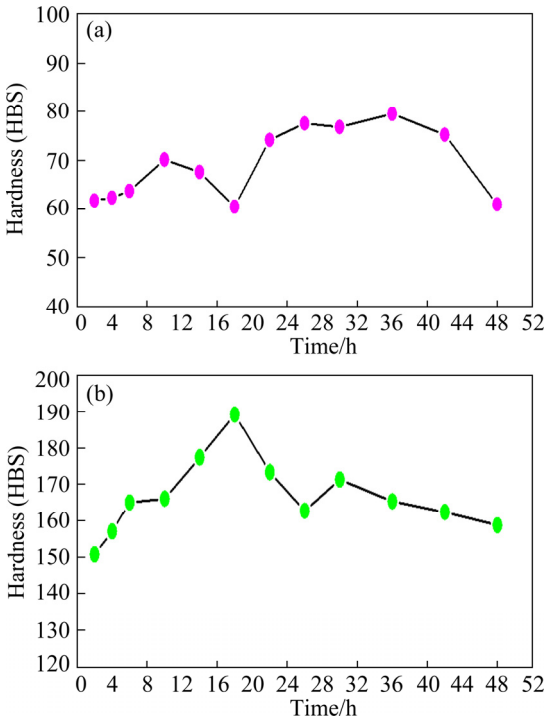

Fig. 8 Aging response of AZ91 alloy (a) and SiC_p/AZ91 composite (b) treated at 175 °C

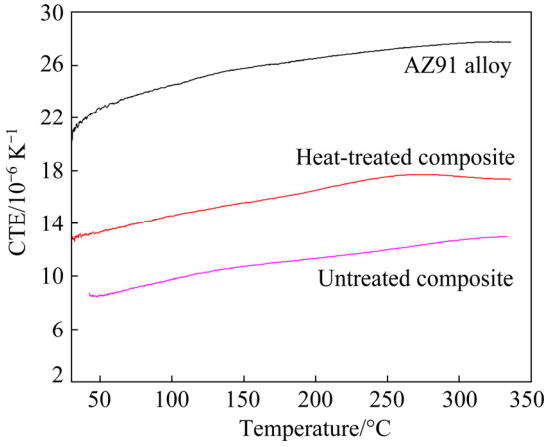

Fig. 9 CTE of AZ91 alloy and SiC_p/AZ91 composite

3.4 Compression test results

The high-temperature compression stress−strain curves of AZ91 and SiCp/AZ91 composites before and after heat treatment are shown in Figs. 10−12. The compression yield strength (CYS) and ultimate compression strength (UCS) of unreinforced magnesium and SiC reinforced composites decreased as temperature increased. All true stress−strain curves were in the work-hardening period at the initial stage followed by a regime of near steady-state flow [31]. The stress−strain curves at the primary stage were governed by work hardening due to the generation and pileup of dislocation [32]. Subsequently, stress gradually decreased as temperature and thermal compression increased possibly because of dynamic recovery and recrystallization. Furthermore, the CYS and

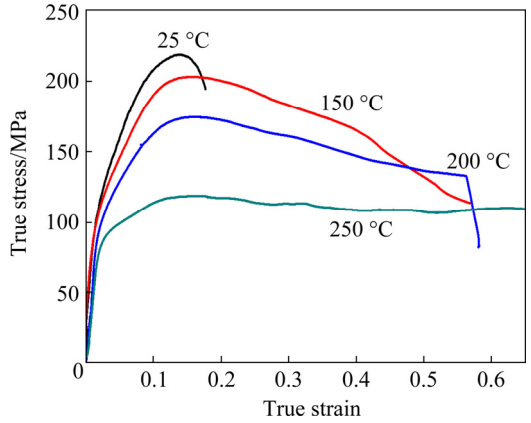

Fig. 10 Typical true stress−strain curves of AZ91 alloy hot compressed at different temperatures

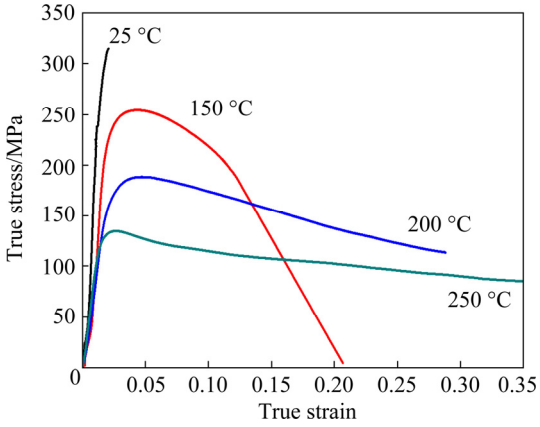

Fig. 11 Typical true stress−strain curves of untreated SiC_p/AZ91 composite hot compressed at different temperatures

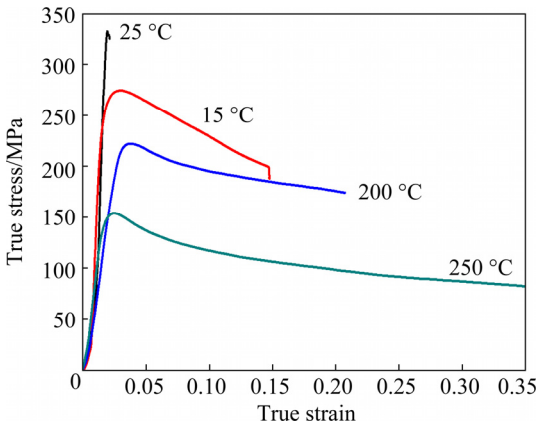

Fig. 12 Typical true stress−strain curves of heat-treated SiC_p/AZ91 composite hot compressed at different temperatures

UCS of the SiC_p/AZ91 composite were higher than those of the AZ91 alloy. Hence, the addition of SiC particles to the AZ91 alloy led to the increased yield strength and UCS.

Figures 13 and 14 respectively show the optical microstructures of the as-cast composite and the heat-treated composite after compression at different temperatures. Similarly, the recrystallized grains preferred to nucleate near SiC. As the deformation and compression deformation temperature increased, the recrystallized grains continued to extend into the original grains. The grain boundaries of the recrystallized grains could also block the migration of dislocations, so new recrystallized grains formed. Lastly, the original grains were completely replaced by recrystallized structures [33]. In Fig. 14, the heat-treated composites compressed at different temperatures underwent aging strengthening, and the precipitates in the composites were more uniform and finer than those in the as-cast composites. Therefore, the high-temperature compressive strength of the heat-treated composites slightly improved compared with that of the as-cast composites.

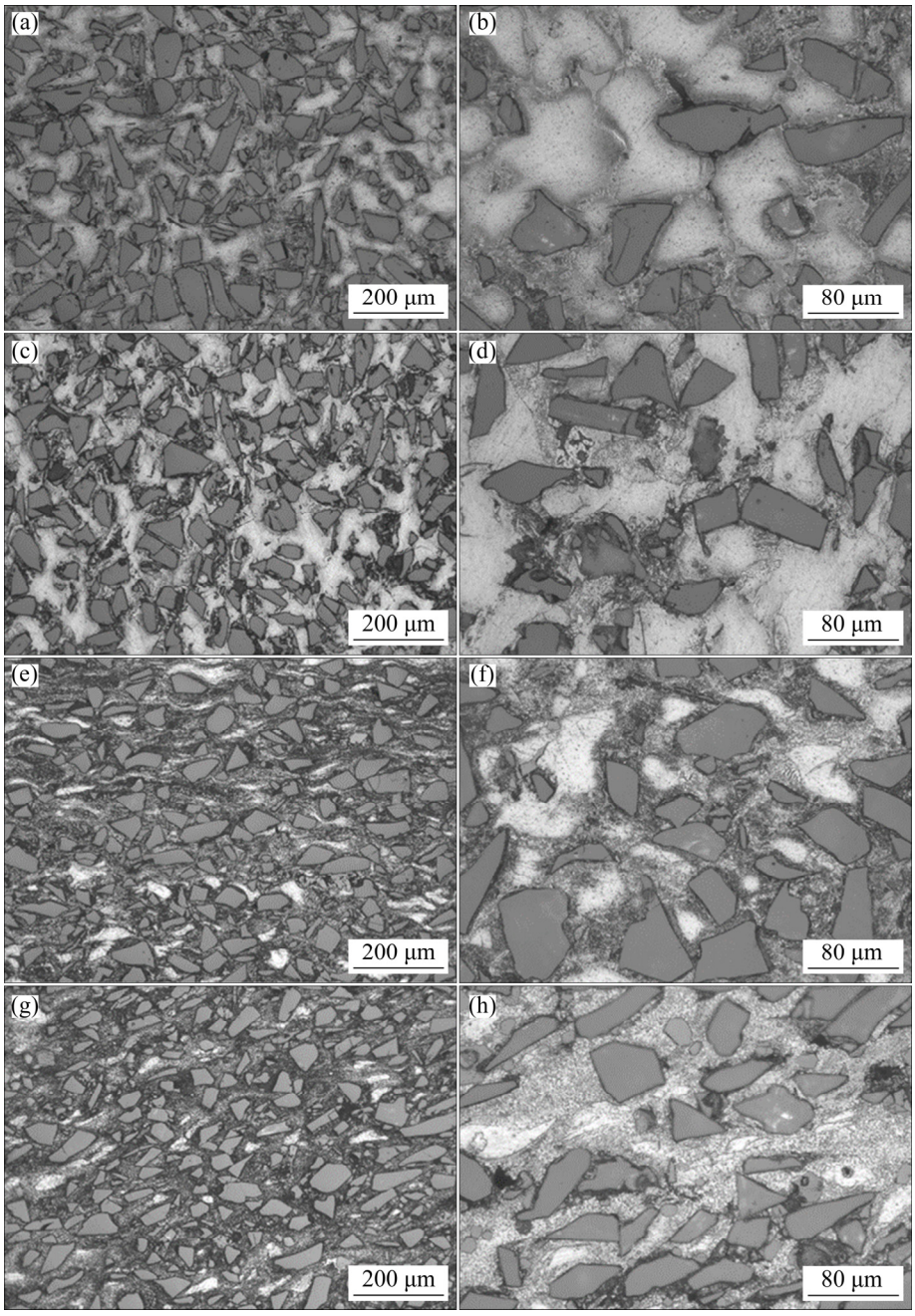

Fig. 13 OM images of as-cast composites compressed at different temperatures: (a, b) 25 °C; (c, d) 150 °C; (e, f) 200 °C; (g, h) 250 °C

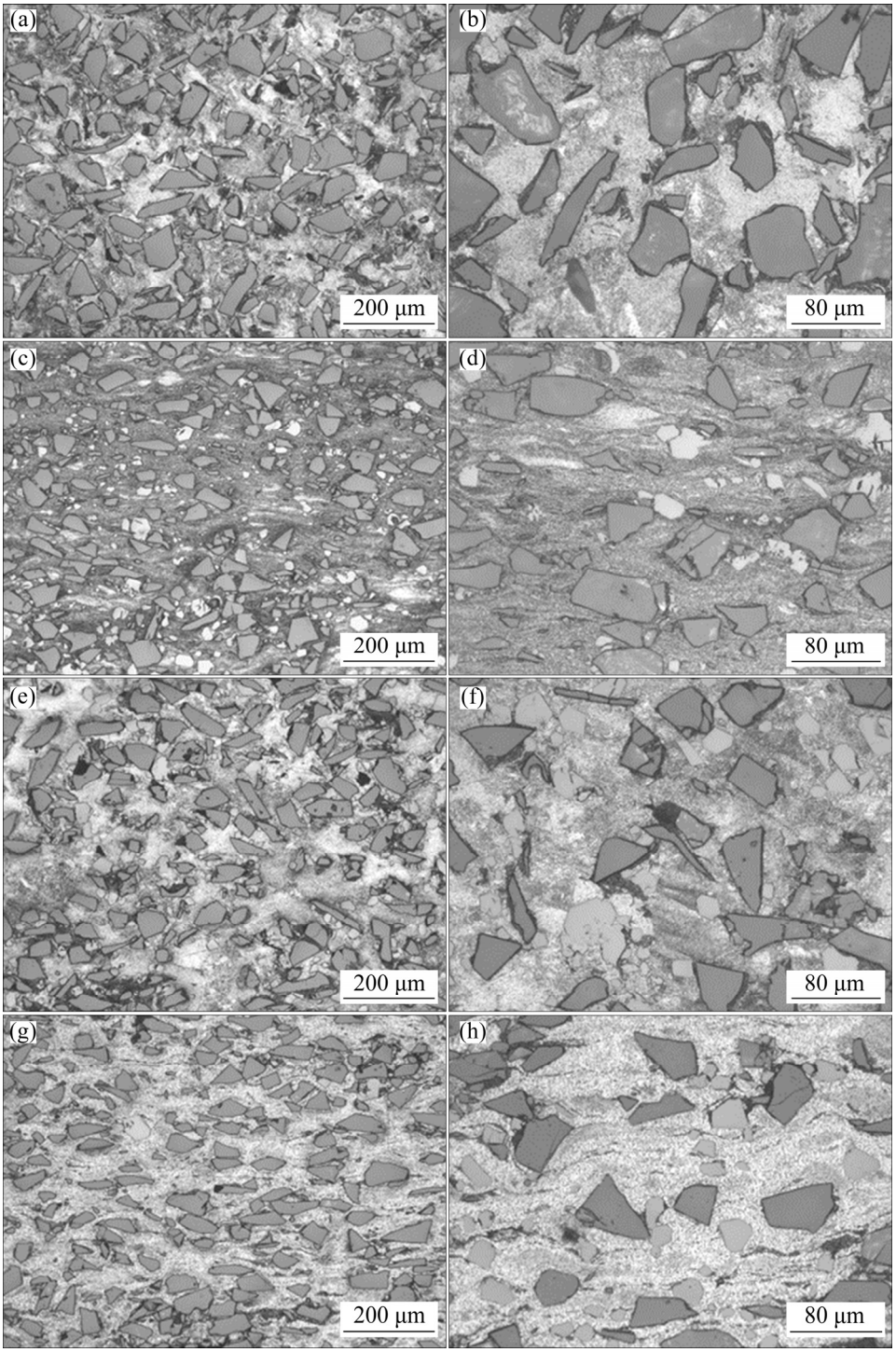

Fig. 14 OM images of heat-treated composites compressed at different temperatures: (a, b) 25 °C; (c, d) 150 °C; (e, f) 200 °C; (g, h) 250 °C

3.5 Wear test results

Figure 15 shows the variation of the wear rate and the specific wear rate with the applied load for the AZ91 and SiC_p/AZ91 composite before and after heat treatment. The wear rate and the specific wear rate were defined by the Archard's law[34]:

$$V/L=K(W/H)=kW \quad (1)$$

where V is the wear volume, L is the sliding distance, W is the applied load, H is the hardness of a sample, K is the Archard's constant, k is the specific wear rate, and V/L is the wear rate. Wear volume was calculated from the ratio of mass loss to density, and wear rate was calculated using a sliding distance and a wear volume. Such relations,

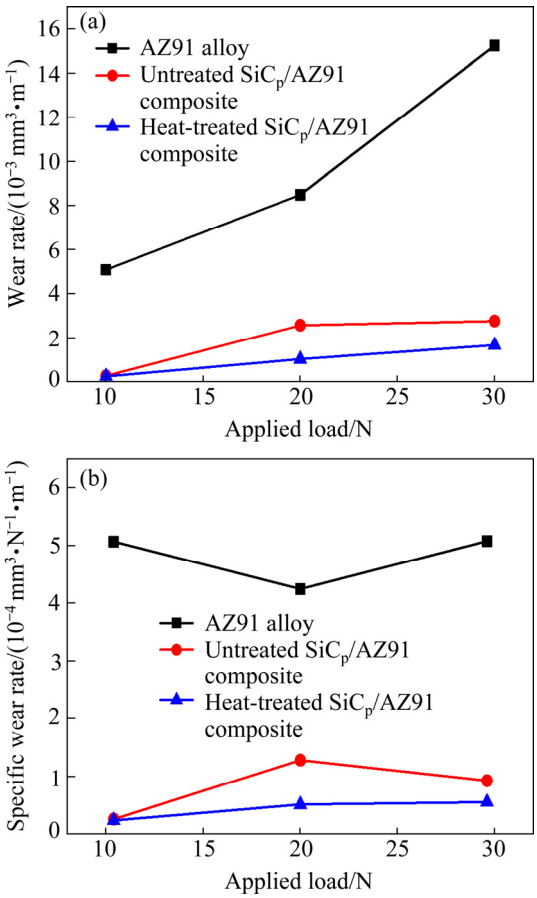

Fig. 15 Variation of wear rate (a) and specific wear rate (b) with applied load for AZ91 alloy and SiC_p/AZ91 composite before and after heat treatment at speed of 1.6 m/s

which were applied by SHARMA et al [35] and LÓPEZ et al [36], are commonly used to calculate the wear parameters. In Fig. 15(a), the volumetric wear rate increased as the load for the unreinforced and reinforced materials increased. Compared with AZ91D magnesium alloy, the wear rate of as-cast composite decreases by 70%−95%, and the wear rate of heat-treated composite decreases by 88%−95%. As the load increased, the interaction between the sample materials and the coupling material was strengthened, thus accelerating their stripping process, and at the same time the friction heat increased, which reduced the yield stress of the material. Consequently, the wear rate increased as the load for the AZ91 and SiC_p/AZ91 composite before and after heat treatment increased. The specific wear rates are shown in Fig. 15(b). The specific wear rate of three materials had no obvious change as the load increased, showing that the primary wear mechanism of the materials did not change obviously when the applied load was 10−30 N. The specific wear rate of the composites increased slightly at loads of 20 and 30 N because of the damage to SiC and the softening of the materials by friction heat. Obviously, the existence of SiC improved the wear behavior of the magnesium matrix for all the applied loads (10, 20, and 30 N). However, the wear resistance of SiC decreased as the load increased. Figure 16 shows that the coefficient of friction (COF) decreased as the load increased. However, the heat-treated composite displayed the highest COF under a load of 30 N because of the different hardness values. The hardness of the untreated composite increased to HBS 90−120 after heat treatment.

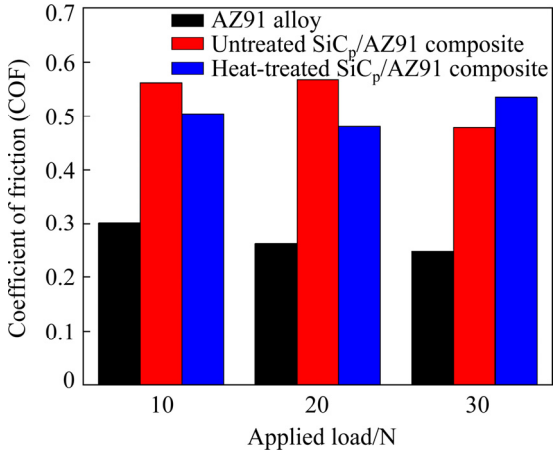

Fig. 16 COF of samples treated at sliding speed of 1.6 m/s

4 Discussion

4.1 Influence of SiC on aging behavior of SiC_p/AZ91 composite

Figure 7 shows the SEM images of $Mg_{17}Al_{12}$, which preferred to nucleate and precipitate near the SiC particles, thereby expanding into a grain. Most precipitates were located at the interface between the particles and the matrix, especially in the area with a high stress-concentration ratio. $Mg_{17}Al_{12}$ precipitated more easily near SiC than at the grain boundaries. NIEH and KARLAK [37] studied the aging hardening of B_4C reinforced 6061Al composites and found that the high density of dislocations accelerate solute diffusion. When dislocations act as channels of solute atoms, the diffusion energy barrier of solute atoms can be effectively reduced, and the interface precipitates can continuously grow and expand into the grain.

During cooling, the CTE of SiC and the matrix alloy greatly differed. SiC and the matrix cannot shrink at the same time. As a result, thermally mismatched stress and increased interfacial dislocation were detected. The lattice distortion energy induced by high density dislocations also provided a driving force for the nucleation and growth of the precipitates. Consequently, $Mg_{17}Al_{12}$ preferentially nucleated around SiC.

With prolonging aging time, a large amount of $Mg_{17}Al_{12}$ precipitates surrounded SiC and extended into the grain, covering the entire observation surface. The high-power SEM image showed that the precipitates near SiC grew more obviously, and their size was larger than that in other regions. The addition of SiC accelerated the aging precipitation of the matrix. Boundary precipitation was accelerated by an increase in dislocation density and grain refinement. SUN et al [38] reported that many defects near grain boundary were observed, such as vacancies and dislocations. These defects served as the rapid diffusion paths of atoms and accelerated the nucleation rate of precipitation [39].

In the composites, $Mg_{17}Al_{12}$ precipitated in two forms, namely, continuous and discontinuous precipitation. The former and the latter primarily occurred inside the grain and at the grain boundary, respectively. The two precipitation modes are competitive. If discontinuous precipitation is sufficient, continuous precipitation becomes less, and vice versa [40]. In the composites, the growth of discontinuous precipitation stopped earlier, and the continuous precipitation was produced on the matrix without discontinuous precipitation. Continuous precipitates had the characteristic of a lamellar structure because of the pinning effect of SiC on grain boundaries in SiC_p/AZ91 [41]. The mobility of the grain boundary is reportedly an important factor in the nucleation and growth of discontinuous precipitation [42,43]. TU and TURNBUL [44] and ZHENG et al [23] indicated that the migration of grain boundary can promote the nucleation and growth of discontinuous precipitation. Moreover, SUN et al [38] reported that the increased SiC content enhanced the pinning effect of SiC. Thus, the addition of SiC inhibited the discontinuous precipitation. Although grain size can be decreased to promote the nucleation and growth of discontinuous precipitates, SiC is important in the inhibition of discontinuous precipitation [38].

4.2 Influence of SiC on mechanical properties of SiC_p/AZ91 composite

4.2.1 High temperature compression strength

As analyzed in Section 3.4, the peak stress of the magnesium alloy and the composite decreased as the compression temperature increased because of the following. First, the critical shear stress required for the sliding of the magnesium alloy matrix decreased as the compression–deformation temperature increased. On the one hand, as temperature increased, the relative distance between atoms increased, the activation energy of atomic layer movement decreased, and the critical deformation force required for deformation decreased. On the other hand, the activation energy of dislocation movement decreased, leading to a relative decrease in the dislocation density and stress [45−47]. Secondly, for the composites, the strengthening of SiC on the magnesium matrix was primarily realized by load transfer. The stress on the magnesium matrix was transferred to SiC through the interface between the reinforcement and the matrix. The bonding strength of the interface was an influencing factor to determine whether the load could be effectively transferred from softer matrix materials to stiffer particles. As compression deformation temperature increased, the strength of the matrix alloy decreased and the plasticity increased. Conversely, as the interfacial bonding strength decreased, cracking at the interface of the reinforcement particles more likely initiated and extended. Furthermore, tempering and recrystallization occurred as the compression temperature increased, and the work hardening weakened [48]. In conclusion, the compressive strength of the magnesium alloy and its composites decreased as compression temperature increased.

The high-temperature compression strength of the heat-treated composite slightly improved compared with that of the untreated composite. Given that the second phase nucleated and grew on dislocations after aging, the dislocation was pinned, thereby improving the deformation resistance of the composite [28]. Accordingly, when the temperature was raised within a certain range, the dislocation inside the heat-treated composite could not be effectively eliminated, leading to the improvement in the compression strength of the composite.

The addition of SiC particles increased the hardness and compressive strength of the composite

compared with those of the AZ91 alloy, which primarily originated from the load transfer strengthening and grain refinement strengthening mechanisms in the composites. Clearly, the addition of SiC particles significantly reduced the grain size of the AZ91 matrix, resulting in the effect of fine grain strengthening. Thus, fine grain strengthening played an important role in SiC particle-reinforced magnesium-matrix composites. As shown in Fig. 9, the CTEs of the AZ91 alloy and the SiC_p/AZ91 composite were 23×10^{-6} and $9\times10^{-6}\,K^{-1}$, respectively. As a result, the CTE of SiC obviously differed from that of the AZ91 alloy. Significant thermal mismatch stress is present inside the composite [49]. ARSENAULT and SHI [50] reported that the thermal mismatch stress caused prismatic punching and dislocation proliferation at the interface. Thus, the strength of the material improved. The theoretical volume fraction of SiC in the composites was 48%, and the size of SiC was small. With the uniform dispersion of reinforcing particles, many particles likely participate in this strengthening mechanism [28,51]. In compression deformation, SiC and the magnesium matrix should be deformed in cooperation because of the difference in the elastic moduli of SiC and the magnesium matrix. Thus, the load was transferred from the soft magnesium matrix to the hard SiC reinforcement. This load transfer mechanism effectively improved the mechanical properties of the materials. Load transfer is related to the interfacial bonding between matrices and reinforcements [18,52]. Figure 5 shows that SiC particles bond well with the magnesium matrix, leading to an efficient load transfer from this matrix to the SiC reinforcement. Thus, the strength of the composite improves.

4.2.2 Wear performance and mechanism

Figure 15 shows that heat treatment slightly affects the wear mechanism, and SiC plays a major role in the wear mechanism. Thus, the AZ91 alloy and the composite without heat treatment are selected to analyze the wear mechanism. The worn surfaces of the samples were investigated through SEM to determine their wear mechanism. The typical surface morphology of the abrasive wear mechanism is the formation of fine grooves and scratch marks [20]. This mechanism was present in the AZ91 alloy under all the loading test conditions. Figure 17 shows the worn surface of AZ91 alloy tested at 10 and 30 N, respectively, at which characteristic grooves can be seen, indicating the main wear mechanism. This result was due to the direct cutting of the hard spot on the surface of the

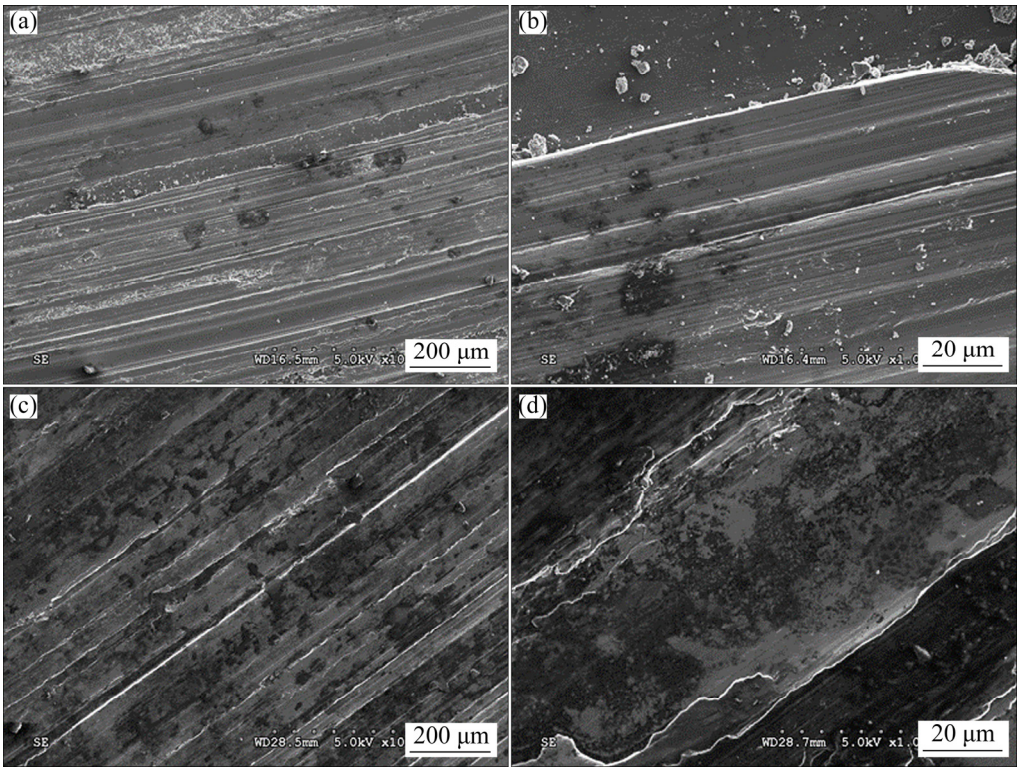

Fig. 17 Worn surfaces of AZ91 alloy treated at different loads: (a, b) 10 N; (c, d) 30 N

coupling materials to the magnesium alloy surface. When the applied load was 10 N, as shown in Fig. 17(b), obvious wear debris was observed in the high-power SEM images. The grooves of the wear surface seemed to widen as the applied load increased to 30 N and became heavy wear occurred, as shown in Figs. 17(c) and (d). In addition to abrasive wear, delamination and adhesion wear were observed. When the load was 30 N, an obvious plastic flow zone existed on the worn surface. The specific wear rate of the AZ91 alloy changed slightly within the range of 10−30 N load, suggesting primarily abrasive wear.

Figure 18 shows the SEM images of the worn surface of the untreated SiC_p/AZ91 composite with different loads and magnification. Figure 18 illustrates obvious differences between the wear surface morphology of the untreated composite and the AZ91 alloy. The directionality of the wear surfaces of the composite was not obvious and had a large number of small planes with a size of approximately 50 μm. In the high-power SEM images (Figs. 18(b) and (d)), the small planes were SiC possibly because SiC was flattened by the coupling material under friction. Figure 18(b) indicates that SiC in the microstructure of the composite was not damaged, and the wear surface was relatively flat as a whole when the applied load was 10 N. As the applied load increased to 20 N, damaged SiC was found. Additionally, compared with the microstructures in Figs. 18(a) and (b), SiC of the wear surface (Figs. 18(c) and (d)) obviously decreased and roughened possibly due to the shedding of SiC during the wear process. As the load increased to more than 20 N, the wear resistance of SiC decreased. The wear resistance of the heat-treated SiC_p/AZ91 composite exceeded that of the untreated composite because the hardness of the heat-treated composite was higher than that of the untreated composite, as shown in Fig. 8(b). Therefore, the wear rate of the heat-treated composite decreased by approximately 8.7%−60% compared with that of the untreated composite. Figure 19 shows the three-dimensional wear morphology of SiC_p/AZ91 (300× magnification). The wear depth at a load of 10 N was shallower than that at 20 N. Figures 19(b) and (d) illustrate many SiC particle platforms. The SiC particle platforms decreased because of the shedding of SiC during the wear process. This finding was consistent with the results of SEM analysis.

Through the analysis of wear parameters and the morphological observation of the worn surface, the wear mechanism diagram of the SiC_p/AZ91 composite was established, as shown in Figs. 20

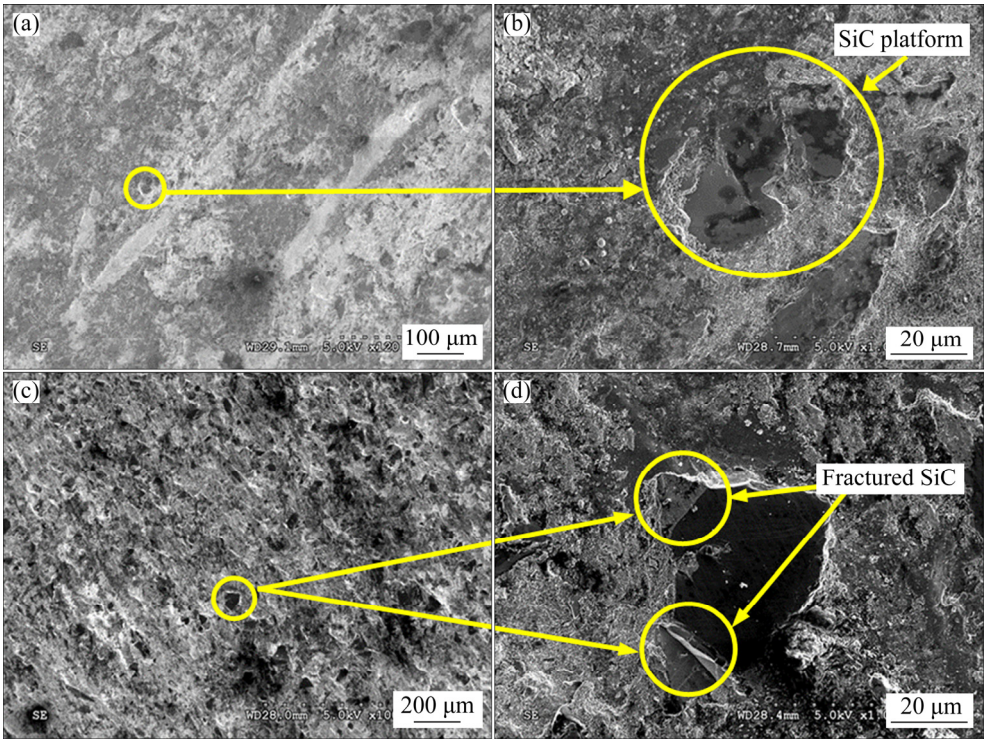

Fig. 18 Worn surfaces of SiC_p/AZ91 composite treated at different loads: (a, b) 10 N; (c, d) 20 N

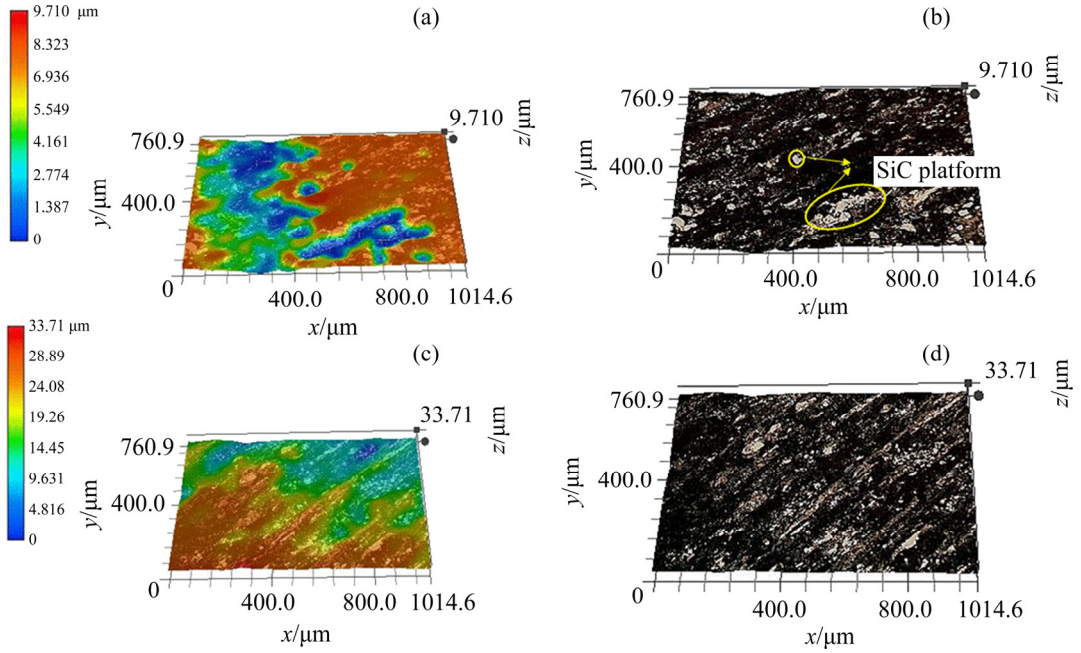

Fig. 19 Three-dimensional microcorrosion morphologies of SiC_p/AZ91 composite at different loads: (a, b) 10 N; (c, d) 20 N

and 21. The anti-attrition mechanism of the SiC_p/AZ91 composite with a high volume fraction was primarily due to the superior wear resistance of SiC. Furthermore, it formed a stable bearing surface to protect the matrix materials during wear. As shown in Fig. 20, at low loads, wear materials primarily formed small particle wear debris and shed from the wear surfaces of the composite. The materials migrated slowly and had a flat wear surface. As the applied load increased to 20 N, as shown in Fig. 21, the internal SiC became gradually exposed to surfaces and formed a bearing surface during wear, causing the stress of SiC and matrix materials to be concentrated on the surface (Fig. 21(b)). SiC with defects was damaged under the action of stress concentration. When worn to a certain extent, SiC and its surrounding magnesium alloy, which satisfied the mechanical condition, fell off from the wear surface because of the poor plasticity of the AZ91 alloy. Therefore, SiC in the composite became partially damaged and underwent shedding. This phenomenon accelerated the damage rate of the stable bearing surface formed by SiC and the wear rate of composite materials (Fig. 21(c)).

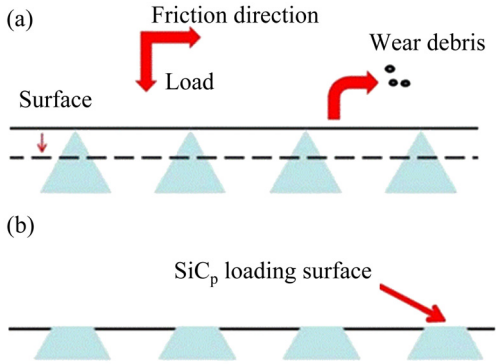

Fig. 20 Wear mechanism maps of SiC_p/AZ91 composite with loads less than 10 N before (a) and after (b) wear

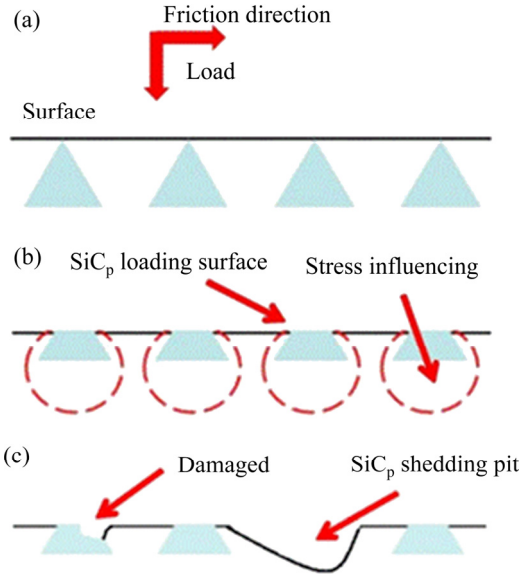

Fig. 21 Wear mechanism maps of SiC_p/AZ91 composite with loads more than 20 N before wear (a), initial stage (b), and after wear (c)

5 Conclusions

(1) The SiC_p/AZ91 composite prepared via vacuum pressure infiltration had a smooth surface and good interfacial bonding. After the aging treatment, the SiC_p/AZ91 composites contained discontinuous and continuous precipitates. High-density dislocations were induced by the mismatch between the CTE of the SiC particles and the AZ91 alloy, and the aging precipitation of the matrix accelerated. The optimum treatment process of the composite was solution treatment at 415 °C for 24 h and aged at 175 °C for 18 h.

(2) The CYS and UCS of the SiC_p/AZ91 composite were higher than those of the AZ91 alloy. After heat treatment, the high-temperature compressive strength of the composites increased slightly. The improvement in the compressive strength of the composites was affected mostly by the SiC particles, which were dominated by load transfer strengthening and grain refinement strengthening mechanisms.

(3) After the load increased, the highest COF of the composites after heat treatment was obtained. The wear rate and specific wear rate of the SiC_p/AZ91 composite were lower than those of the AZ91 alloy. The existence of SiC improved the wear mechanism of the magnesium matrix under a specific load. A stable support surface-protecting matrix formed during the wear process because of the excellent wear resistance of SiC. However, the wear resistance of SiC decreased as the load increased to 20 N.

Acknowledgments

The authors are grateful for the financial supports from the National Natural Science Foundation of China (Nos. U1810208, 51575230), and the Science and Technology Development Program of Jilin Province, China (No. 20190302059GX).

References

[1] BAI Pu-cun, DONG Tai-shang, HOU Xiao-hu, ZHAO Chun-wang, XING Yong-ming. Microstructure and mechanical properties of spray-deposited Mg−12.55Al−3.33Zn−0.58Ca−1Nd alloy [J]. Materials Characterization, 2010, 61: 756−760.

[2] YANG Zhen-quan, MA Ai-bin, LIU Huan, SONG Dan, WU Yu-na, YUAN Yu-chun, JIANG Jing-hua, SUN Jia-peng. Managing strength and ductility in AZ91 magnesium alloy through ECAP combined with prior and post aging treatment [J]. Materials Characterization, 2019, 152: 213−222.

[3] FU Yan-tao, SUN Jia-peng, YANG Zhen-quan, XU Bing-qian, HAN Jing, CHEN Yi-fei, JIANG Jing-hua, MA Ai-bin. Aging behavior of a fine-grained Mg−10.6Gd−2Ag alloy processed by ECAP [J]. Materials Characterization, 2020, 165: 110398.

[4] MORDIKE B L, EBERT T. Magnesium properties−applications−potential [J]. Materials Science and Engineering A, 2001, 302: 37−45.

[5] LUO A A. Magnesium casting technology for structural applications [J]. Journal of Magnesium and Alloys, 2013, 1: 2−22.

[6] BAGHERI B, ABBASI M, ABDOLLAHZADEH A, MIRSALEHI S E. Effect of second-phase particle size and presence of vibration on AZ91/SiC surface composite layer produced by FSP [J]. Transactions of Nonferrous Metals Society of China, 2020, 30: 905−916.

[7] GUO Su-qing, WANG Ri-chu, PENG Chao-qun, CAI Zhi-yong, DONG Cui-ge. Microstructures and mechanical properties of Ni-coated SiC particles reinforced AZ61 alloy composites [J]. Transactions of Nonferrous Metals Society of China, 2019, 29: 1854−1863.

[8] HASSAN S F, PARAMSOTHY M, PATEL F, GUPTA M. High temperature tensile response of nano-Al_2O_3 reinforced AZ31 nanocomposites [J]. Materials Science and Engineering A, 2012, 558: 278−284.

[9] SAHOO B N, PANIGRAHI S K. Effect of in-situ (TiC−TiB_2) reinforcement on aging and mechanical behavior of AZ91 magnesium matrix composite [J]. Materials Characterization, 2018, 139: 221−232.

[10] ANASORI B, CASPI E N, BARSOUM M W. Fabrication and mechanical properties of pressureless melt infiltrated magnesium alloy composites reinforced with TiC and Ti_2AlC particles [J]. Materials Science and Engineering A, 2014, 618: 511−522.

[11] RASHAD M, PAN F, ZHANG J, ASIF M. Use of high energy ball milling to study the role of graphene nanoplatelets and carbon nanotubes reinforced magnesium alloy [J]. Journal of Alloys and Compounds, 2015, 646: 223−232.

[12] ZHOU Xia, LIU Zi-fan, SU Feng, FAN Ya-fu. Magnesium composites with hybrid nano-reinforcements: 3D simulation of dynamic tensile response at elevated temperatures [J]. Transactions of Nonferrous Metals Society of China, 2021, 31: 636−647.

[13] SANKARANARAYANAN S, HABIBI M K, JAYALAKSHMI S, JIA AI K, ALMAJID A, GUPTA M. Nano-AlN particle reinforced Mg composites: Microstructural and mechanical properties [J]. Journal of Materials Science and Technology, 2015, 31: 1122−1131.

[14] SARAVANAN R A, SURAPPA M K. Fabrication and characterisation of pure magnesium 30 vol.% SiC_p particle composite [J]. Materials Science and Engineering A, 2000, 276: 108−116.

[15] VISWANATH A, DIERINGA H, AJITH KUMAR K K, PILLAI U T S, PAI B C. Investigation on mechanical

properties and creep behavior of stir cast AZ91-SiC_p composites [J]. Journal of Magnesium and Alloys, 2015, 3: 16−22.

[16] GANGULY S, MONDAL A K. Influence of SiC nanoparticles addition on microstructure and creep behavior of squeeze-cast AZ91-Ca−Sb magnesium alloy [J]. Materials Science and Engineering A, 2018, 718: 377−389.

[17] RASHAD M, PAN F, LIN D, ASIF M. High temperature mechanical behavior of AZ61 magnesium alloy reinforced with graphene nanoplatelets [J]. Materials and Design, 2016, 89: 1242−1250.

[18] TURAN M E, SUN Y, AKGUL Y. Mechanical, tribological and corrosion properties of fullerene reinforced magnesium matrix composites fabricated by semi powder metallurgy [J]. Journal of Alloys and Compounds, 2018, 740: 1149−1158.

[19] LIM C Y H, LIM S C, GUPTA M. Wear behaviour of SiC_p-reinforced magnesium matrix composites[J]. Wear, 2003, 255: 629−637.

[20] GARCÍA-RODRÍGUEZ S, TORRES B, MAROTO A, LÓPEZ A J, OTERO E, RAMS J. Dry sliding wear behavior of globular AZ91 magnesium alloy and AZ91/SiC_p composites [J]. Wear, 2017, 390/391: 1−10.

[21] DUTTA I, ALLEN S M, HAFLEY J L. Effect of reinforcement on the aging response of cast 6061 Al−Al_2O_3 particulate composites [J]. Metallurgical Transactions A, 1991, 22: 2553−2563.

[22] KNOWLES D M, KING J E. The influence of ageing on fatigue crack growth in SiC-particulate reinforced 8090 [J]. Acta Metallurgica et Materialia, 1991, 39: 793−806.

[23] ZHENG M Y, WU K, KAMADO S, KOJIMA Y. Aging behavior of squeeze cast SiC_w/AZ91 magnesium matrix composite [J]. Materials Science and Engineering A, 2003, 348: 67−75.

[24] DONG Cui-ge, WANG Ri-chu, CHEN Yi-xin, WANG Xiao-feng, PENG Chao-qun, ZENG Jing. Near-net shaped Al/SiC_p composites via vacuum-pressure infiltration combined with gelcasting [J]. Transactions of Nonferrous Metals Society of China, 2020, 30: 1452−1462.

[25] ZHU Jing-bo, WANG Fu-chi, WANG Yang-wei, ZHANG Bo-wen, WANG Lu. Interfacial structure and stability of a co-continuous SiC/Al composite prepared by vacuum-pressure infiltration [J]. Ceramics International, 2017, 43: 6563−6570.

[26] XIE Bin, WANG Xiao-gang, HUA Xiao-hu, YI Da-wei. Process and performance of β-SiC_p/Al prepared by bot-tom-vacuum pressureless infiltration [J]. Rare Metal Materials and Engineering, 2014, 43: 2089−2094.

[27] XIONG Bo-wen, YU Huan, XU Zhi-feng, YAN Qing-song, CAI Chang-chun. Fabrication of SiC particulate reinforced AZ91D composite by vacuum-assisted pressure infiltration technology [J]. Journal of Alloys and Compounds, 2011, 509: L279−L283.

[28] WANG X J, HU X S, LIU W Q, DU J F, WU K, HUANG Y D, ZHENG M Y. Aging behavior of as-cast SiC_p/AZ91 Mg matrix composites [J]. Materials Science and Engineering A, 2017, 682: 491−500.

[29] YI Y S, MENG Y, LI D Q, SUGIYAMA S, YANAGIMOTO J. Partial melting behavior and thixoforming properties of extruded magnesium alloy AZ91 with and without addition of SiC particles with a volume fraction of 15% [J]. Journal of Materials Science and Technology, 2018, 34: 1149−1161.

[30] JIANG Yan-bin, GUAN Lei, TANG Guo-yi, ZHANG Zhi-hao. Improved mechanical properties of Mg−9Al−1Zn alloy by the combination of aging, cold-rolling and electropulsing treatment [J]. Journal of Alloys and Compounds, 2015, 626: 297−303.

[31] WANG X J, HU X S, WU K, DENG K K, GAN W M, WANG C Y, ZHENG M Y. Hot deformation behavior of SiC_p/AZ91 magnesium matrix composite fabricated by stir casting [J]. Materials Science and Engineering A, 2008, 492: 481−485.

[32] HAN G M, HAN Z Q, LUO A, LIU B C. Microstructure characteristics and effect of aging process on the mechanical properties of squeeze-cast AZ91 alloy [J]. Journal of Alloys and Compounds, 2015, 641: 56−63.

[33] PONGE D, GOTTSTEIN G. Necklace formation during dynamic recrystallization: Mechanisms and impact on flow behavior [J]. Acta Materialia, 1998, 46: 69−80.

[34] ARCHARD J F. Contact and rubbing of flat surfaces [J]. Journal of Applied Physics, 1953, 24(8): 981−988.

[35] SHARMA S C, GIRISH B M, SOMASHEKAR D R, SATISH B M, KAMATH R. Sliding wear behaviour of zircon particles reinforced ZA-27 alloy composite materials [J]. Wear, 1999, 224: 89−94.

[36] LÓPEZ A J, RODRIGO P, TORRES B, RAMS J. Dry sliding wear behaviour of ZE41A magnesium alloy [J]. Wear, 2011, 271: 2836−2844.

[37] NIEH T G, KARLAK R F. Aging characteristics of B_4C-reinforced 6061-aluminum [J]. Scripta Metallurgica, 1984, 18: 25−28.

[38] SUN Xue-fei, WANG Cui-ju, DENG Kun-kun, KANG Jin-wen, BAI Yan, NIE Kai-bo, SHANG Shuan-jun. Aging behavior of AZ91 matrix influenced by 5 μm SiC_p: Investigation on the microstructure and mechanical properties [J]. Journal of Alloys and Compounds, 2017, 727: 1263−1272.

[39] RAUBER C, LOHMULLER A, OPEL S, SINGER R F. Microstructure and mechanical properties of SiC particle reinforced magnesium composites processed by injection molding [J]. Materials Science and Engineering A, 2011, 528: 6313−6323.

[40] ZHANG M X, KELLY P M. Crystallography of $Mg_{17}Al_{12}$ precipitates in AZ91D alloy [J]. Scripta Materialia, 2003, 48: 647−652.

[41] DENG K K, WANG X J, ZHENG M Y, WU K. Dynamic recrystallization behavior during hot deformation and mechanical properties of 0.2 μm SiC_p reinforced Mg matrix composite [J]. Materials Science and Engineering A, 2013, 560: 824−830.

[42] DULY D, SIMON J P, BRECHET Y. On the competition between continuous and discontinuous precipitations in binary Mg−Al alloys [J]. Acta Metallurgica et Materialia, 1995, 43: 101−106.

[43] DULY D, BRECHET Y, CHENAL B. Macroscopic kinetics of discontinuous precipitation in a Mg−8.5wt.% Al alloy [J]. Acta Metallurgica et Materialia, 1992, 40: 2289−2300.

[44] TU K N, TURNBUL D. Morphology of cellular precipitation of tin from lead−tin bicrystals-II [J]. Acta Metallurgica, 1967, 15: 369−376.
[45] ZHOU S S, ZHOU H F, SHANG S J, LI J C, KANG G F, DENG K K. Hot deformation behaviour of Mg−Al−Zn alloys [J]. Materials Research Innovations, 2014, 18: 654−660.
[46] HUMPHREYS F J, HATHERLY M. Recrystallization and related annealing phenomena [M]. Oxford: Elsevier, 2004.
[47] ZHOU S S, DENG K K, LI J C, NIE K B, XU F J, ZHOU H F, FAN J F. Hot deformation behavior and workability characteristics of bimodal size SiC_p/AZ91 magnesium matrix composite with processing map [J]. Materials and Design, 2014, 64: 117−184.
[48] ZHOU S S, DENG K K, LI J C, SHANG S J, LIANG W, FAN J F. Effects of volume ratio on the microstructure and mechanical properties of particle reinforced magnesium matrix composite [J]. Materials and Design, 2014, 63: 672−677.
[49] LIAO Wen-jun, YE Bing, ZHANG Li, ZHOU Hao, GUO Wei, WANG Qu-dong, LI Wen-zhen. Microstructure evolution and mechanical properties of SiC nanoparticles reinforced magnesium matrix composite processed by cyclic closed-die forging [J]. Materials Science and Engineering A, 2015, 642: 49−56.
[50] ARSENAULT R J, SHI N. Dislocation generation due to differences between the coefficients of thermal expansion [J]. Materials Science and Engineering A, 1986, 81: 175−187.
[51] KIM W J, JEONG H G, JEONG H T. Achieving high strength and high ductility in magnesium alloys using severe plastic deformation combined with low-temperature aging [J]. Scripta Materialia, 2009, 61: 1040−1043.
[52] RASHAD M, PAN F, TANG A, ASIF M. Effect of graphene nanoplatelets addition on mechanical properties of pure aluminum using a semi-powder method [J]. Progress in Natural Science, 2014, 24: 101−108.

真空压力浸渗制备 SiC_p/AZ91 复合材料的显微组织、力学性能和磨损行为

管志平[1,2]，李明宇[1,2]，夏凯欣[2]，李志刚[2]，高 丹[2]，赵 泼[2]，马品奎[2]，宋家旺[1]

1. 吉林大学 汽车仿真与控制国家重点实验室，长春 130022；
2. 吉林大学 材料科学与工程学院，长春 130022

摘 要：采用真空压力浸透法制备 SiC_p/AZ91 复合材料，研究其显微组织、力学性能和耐磨性。结果表明，SiC 颗粒均匀分布于金属基体中，并与基体界面结合良好。$Mg_{17}Al_{12}$ 相在 SiC 颗粒附近优先析出，SiC 与 AZ91 基体的热膨胀系数失配导致高密度位错的产生，加速基体的时效析出。与 AZ91 合金相比，SiC 颗粒的加入提高了复合材料的硬度和抗压强度，这主要是由于载荷传递强化和晶粒细化强化机制。此外，由于 SiC 具有优异的耐磨性，在磨损过程中形成稳定的支撑面保护基体。

关键词：镁基复合材料；SiC 颗粒；真空压力浸透；时效行为；磨损

(Edited by Xiang-qun LI)